INTERNATIONAL JOURNAL OF CLIMATOLOGY
Int. J. Climatol. (2016)
Published online in Wiley Online Library
(wileyonlinelibrary.com) DOI: 10.1002/joc.4581

RMetS
Royal Meteorological Society

ENSO impacts on temperature over South Korea

Jai Hong Lee* and Pierre Y. Julien

Department of Civil and Environmental Engineering, Colorado State University, Fort Collins, CO, USA

ABSTRACT: The climatic impact of the two phases (warm/cold) of ENSO phenomena on monthly temperature patterns over South Korea is examined based on the composite and harmonic analysis. The core regions, namely the north-east region and the south-west region, were identified with a high-level spatial coherence and temporal consistency, which represent the geographical extent and magnitude of the response of the ENSO forcing to the temperature patterns. For the both regions, the temperature anomalies in El Nino year are below normal for summer through fall of the ENSO year and above normal for winter through spring of the following year. The spatial coherence rates of each region are 0.95, 0.97 and the temporal consistency rates are 0.70/0.70 (cold/warm) and 0.70/0.80 (cold/warm), respectively. On the other hand, in case of the cold events, the temperature anomalies for the both regions are above normal for summer through fall of the episode year and below normal for winter through spring of the following year. The spatial coherence rates of each region are 0.98, 0.99 and the temporal consistency rates are 1.00/0.78 (warm/cold) and 0.89/0.78 (warm/cold), respectively. According to the comparative analyses for both extreme episodes in two core regions, the El Niño/La Niña–temperature relationships show reverse patterns of sign, negative–positive and positive–negative temperature anomalies, respectively. Based on the results of annual cycle analysis, Mann–Whitney U test and cross-correlation analysis, the cold–warm anomalies during the warm event years are more remarkable and significant than the warm–cold departures during the cold event years. Consequently, the climatic teleconnective pattern between the extreme phase of SO and mid-latitude temperature is identified over South Korea.

KEY WORDS ENSO; El Niño; La Niña; Southern Oscillation; temperature

Received 22 May 2015; Revised 30 October 2015; Accepted 2 November 2015

1. Introduction

The typical examples of large-scale natural climate variability are El Niño and La Niña characterized by the unusual wide-ranging warming and cooling of the sea surface temperature (SST) ranging from the central to eastern tropical Pacific Ocean. These two types of fluctuations of the SST are interactive with the Southern Oscillation (SO) defined as an atmospheric circulation of pressure over the eastern-western equatorial Pacific with a periodic seesaw pattern. Originally, El Niño and La Niña were considered as the oceanic phenomena, while SO was regarded as the atmospheric variation. The interaction of the above oceanic fluctuation and atmospheric oscillation defines the El Niño/Southern Oscillation (ENSO), well known as a naturally occurring phenomenon involving fluctuating ocean temperatures over the central-eastern tropical Pacific Ocean, coupled with changes in the atmosphere (WMO, 2014).

Since the first approaches by Walker (1923) and Walker and Bliss (1932) to the impact of the extreme phase of SO on the variation of Indian monsoon rainfall, in the recent decades many global scale studies associated with ENSO showed remarkable climatic link between temperature patterns and both warm and cold phases of Southern Oscillation (SO) in various areas of the world. Berlage (1966) showed the statistically significant correlations between climate indices (SO) and temperature patterns in some regions of the globe, and Rasmusson and Carpenter (1983) revealed evidence of significant linkage between the evolution of the ENSO and anomalies in surface temperature over the tropical Pacific. Moreover, more recent studies by Bradley *et al.* (1987), Kiladis and Diaz (1989), and Halpert and Ropelewski (1992), revealed noticeable ENSO–temperature relationships with the identification of the seasons and regions having a consistent response of the warm and cold phases of SO to the temperature pattern over the several regions of the globe.

Much of the regional scale work relating the extreme phase of SO to hydrometeorological parameters over low and middle latitude by van Loon and Madden (1981), Ropelewski and Halpert (1986), Redmond and Koch (1991), and Kiladis and van Loon (1988) found plausible evidence of strong and coherent links between ENSO and temperature patterns. In detail, for mid-latitude regions, the importance of the ENSO–temperature relationships is emphasized in several studies. The climatic relationship between low and high phases of SO and North American temperature have been investigated by Ropelewski and Halpert (1986) and Kiladis and Diaz (1989).

In South Korea, several recent studies exist concerning temperature patterns associated with the ENSO events

* Correspondence to: J. H. Lee, Department of Civil and Environmental Engineering, Colorado State University, 1320 Campus Delivery, Fort Collins, CO 80523, USA. E-mail: june.lee@colostate.edu

(El Niño/La Niña). Ha (1995) showed significant relationship between the interannual variability of Seoul wintertime air temperature and the sea surface temperature (SST) using cross-correlation analysis. Ahn *et al.* (1997) examined the linkage of the winter and summer air temperatures over five Korean metropolises and SST patterns in western-central Pacific Ocean, and concluded that SST anomalies of a particular part of tropical Pacific could be a good index for a long-term forecast of a certain variables. Lee (1998) applied harmonic analysis to investigate the relationship between both extreme phases of SO and temperature/precipitation over South Korea. Kang (1998) investigated the climatic link between El Niño and Korean climate variability based on spectrum analysis, and Min and Yang (1998) documented the impacts of El Niño and La Niña on winter meteorology in Korea. Cha *et al.* (1999) investigated the relationship between El Niño/La Niña events and the climate in Korea using synoptic data and ECMWF (European Centre for Medium-range Weather Forecasts) grid data, and showed that El Niño forcing has a tendency to modulate the temperature over Korea by enhancing or suppressing with respect to seasons.

As seen from the above, the majority of previous global/regional scale studies have focused on mostly the Pacific Rim countries. These studies revealed the significant teleconnection between the ENSO events and hydrometeorological variables in the lower to mid-latitudes; however, the impact of El Nino and La Nina events on the mid to high latitudes is not clear. The global scale study by Halpert and Ropelewski (1992) showed significant ENSO–temperature relationship in some regions over the globe, with some potential for the signal over the East Asia. According to a visual inspection of station locations in the above study, the existence of the ENSO signals is not clearly identified in South Korea due to the limitation of data coverage. This indicates the need for a diagnostic investigation on the impact of ENSO forcing over South Korea based on adequate and sufficient data set.

The main objectives of this investigation are to : identify coherent, consistent, and significant response of the warm/cold extreme phase of the SO (El Niño/La Niña) to the temperature patterns over South Korea, using a composite and harmonic analysis based on the improved description of the magnitude, phase, and geographical extent of the ENSO-related temperature response; examine the comparison between El Niño and La Niña–temperature relationships with the viewpoint of intensity and trend of the significant responses, by comparative analyses such as an annual cycle analysis, a Mann–Whitney U hypothesis test, and a cross-correlation analysis.

2. Data set and methodology

2.1. Data set

The time series of monthly temperature records applied in this analysis are based on 76 stations distributed all over South Korea. The source of these data set is Korea Meteorological Administration which is a governmental organization under the Ministry of Environment. The time series extend from 1904 to 2014 and cover more than about 20 episodes of El Niño and La Niña. Not only the meteorological stations with missing data for more than a season were excluded, but also the stations with less than 42 years of data or spanning less than nine ENSO events were ruled out from the analysis. Finally, by taking the temporal persistency and spatial distribution into consideration, a subset of 60 gauging stations are selected in this study (Figure 1). The longest time series extend from 1904 to 2014 and span 27 warm (or 20 cold) episodes, while all 60 stations have at least more than 42 years of monthly temperature data spanning 10 warm (or 9 cold) episodes. Following a suggestion of Halpert and Ropelewski (1992), data transformation, ENSO composite, harmonic analysis, identification of candidate region, and aggregate composite are based on the entire period for the monthly temperature data of 60 meteorological stations over South Korea. Meanwhile, the index time series (ITS) are based on the period from 1973 to 2014 available in all 60 stations in order to average regionally and temporally the temperature data over the all stations.

In order to detect a consistent influence of ENSO episodes on temperature pattern over South Korea, a wide set of ENSO events is selected by a comprehensive range of criteria based on the definition and classification by Quinn *et al.* (1978), Rasmusson and Carpenter (1983), Ropelewski and Halpert (1987, 1989),

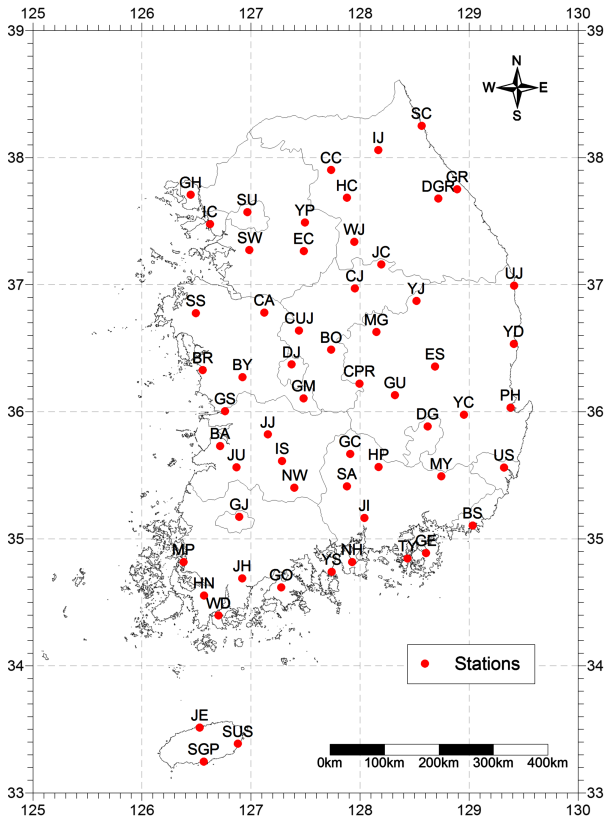

Figure 1. Stations used for temperature indices.

Table 1. List of the ENSO episode years included in this study.

El Niño years	La Niña years
1905, 1911, 1914, 1918, 1923, 1925, 1930, 1932, 1939, 1941, 1951, 1953, 1957, 1963, 1965, 1969, 1972, 1976, 1982, 1986, 1991, 1994, 1997, 2002, 2004, 2006, and 2009.	1910, 1915, 1917, 1924, 1928, 1938, 1950, 1955, 1964, 1971, 1973, 1975, 1985, 1988, 1995, 1998, 2000, 2005, 2007, and 2010.

Kiladis and Diaz (1989), and Trenberth (1997). The overall ENSO years applied in this analysis are shown in Table 1.

As a method of representing large-scale climate fluctuation over the Pacific Ocean, a climatic index known as the Southern Oscillation index (SOI) is employed following the approach of Ropelewski and Halpert (1986, 1987), Kahya and Dracup (1993, 1994), and Jin *et al.* (2005). The time series of SOI are calculated using the difference of the standardized anomalies of the sea level atmospheric pressures between the Tahiti and Darwin, Australia. The time series of SOI calculated by the NOAA Climate Prediction Center is applied in the present study.

2.2. Methodology

Figure 2 shows the schematic description for the overall methodology used in this study, based on the approach of Ropelewski and Halpert (1986). The detailed procedures of the methodology comprise primarily three stages, namely, data processing, analytical method application, and comparative analysis. The first stage is intended for transforming the original raw data into an appropriate data format such as Standardized Temperature index (STI), non-exceedance probability series, categorized SOI, and modular coefficients. The second stage is to detect candidate regions and confirm core regions based on composite and harmonic analysis. Finally the last stage is focused on the comparative interpretation on El Niño– and La Niña–temperature relationships using annual cycle analysis, Mann–Whitney U test, and cross-correlation analysis.

2.2.1. *Data processing*

For the composite and harmonic analysis to identify the ENSO response to the local temperature patterns, the original monthly temperature data were transformed into STI, which is produced by applying the calculation method of Standardized Precipitation index (SPI) to temperature data. The SPI estimated by McKee *et al.* (1993), which is recommended by World Meteorological Organization (WMO, 2014), is a probability index based on statistical fit and standardization. To calculate the SPI, McKee *et al.* (1993) fitted a gamma distribution to the precipitation histogram. The cumulative density function (CDF) of the fitted distribution is then transformed to the CDF of the standard normal distribution by the equal-probability transformation. The transformed standard deviate is the SPI for the given data with a mean of zero and standard deviation of unity.

In this study, the monthly temperature data (Fahrenheit) of 60 meteorological stations over South Korea are fitted to a normal distribution for calculating the STI following the calculation method of SPI by McKee *et al.* (1993). The fitted distribution, subsequently, is transformed into a CDF of the standard normal distribution. The STI time series, which can be used in the composite and harmonic analysis, are calculated using the resulting standard deviates of the transformed CDF with zero mean and unit variance. This

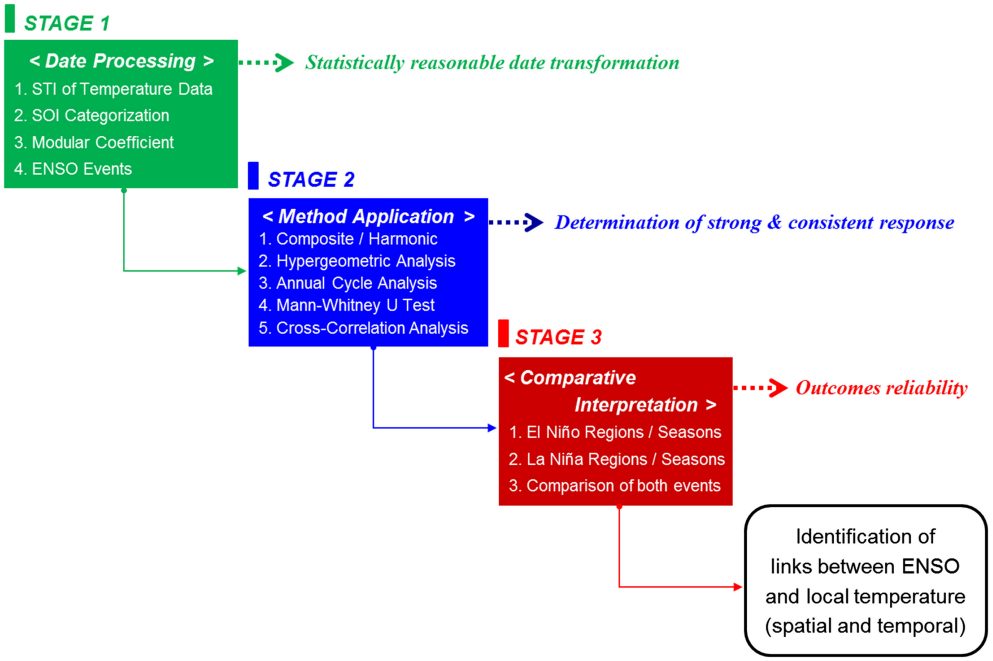

Figure 2. Flowchart presentation of the empirical methodology consisting of three stages.

probability index is not only fairly easy to compute since the input data is only one variable, but also simple to compare in terms of space and time due to being provided as dimensionless index values. Also, it is spatially consistent and analytical for probabilistic process (Guttman, 1998).

In order to examine the quantitative and significant impact of the SOI on temperature patterns over South Korea, the cross-correlation coefficients (CCC) are calculated between the categorized SOI and the seasonal temperature series. In this analysis, four seasonal averages of SOI and temperature data are formed according to 3 months averaged seasons, which are defined as: December to February, March to May, June to August, and September to November. Prior to the correlation analysis, the temperature data for each individual season are converted into non-exceedance probability time series to deal with the disparities among stations and to get rid of periodicities in the time series. The non-exceedance probability can be obtained using the Weibull plotting position formula. The entire temperature data for each individual season are ranked from the smallest amount to the largest amount, and then divided by $n+1$ (n is the number of data). Subsequently, the resulting associated values are the non-exceedance probability time series for each season. In addition, the SOI is classified into five categories based on the magnitudes of each data following the suggestion of Jin *et al.* (2005). The SOI values are assigned to each category which is grouped into five levels in accordance with the magnitude: Strong La Niña ($SOI > 2$), Weak La Niña ($1 < SOI \leq 2$), Normal Phase ($-1 \leq S \leq 1$), Weak El Niño ($-2 \leq SOI < -1$), and Strong El Niño ($SOI < -2$).

For annual cycle analysis, the monthly temperature data are converted to a modular coefficient to remove the effect of dispersed mean and variance values, which is a method to express monthly temperature values according to the percent of mean annual values. The time series of modular coefficient are obtained by the proportion of the original temperature data to the monthly mean data, which are averaged over the total data series, to place all stations on a same basis with invariable condition of the cyclic feature of the values, simultaneously.

2.2.2. *Method application*

For composite analysis, as an approach to describe the general patterns of the ENSO-related temperature behaviour, the 24-month ENSO composites are formed for each station, starting from the July of previous year of the events designated as July (−), through the event years designated as (0), to the June of subsequent year of the events designated as June (+), based on the method described by Ropelewski and Halpert (1986). By means of averaging the converted temperature data for the all proposed ENSO episodes on an equal basis, the final ENSO composite is calculated.

The time series of 24-month ENSO composite are subjected to a harmonic analysis representing a periodic function by the summation and integration of a series of

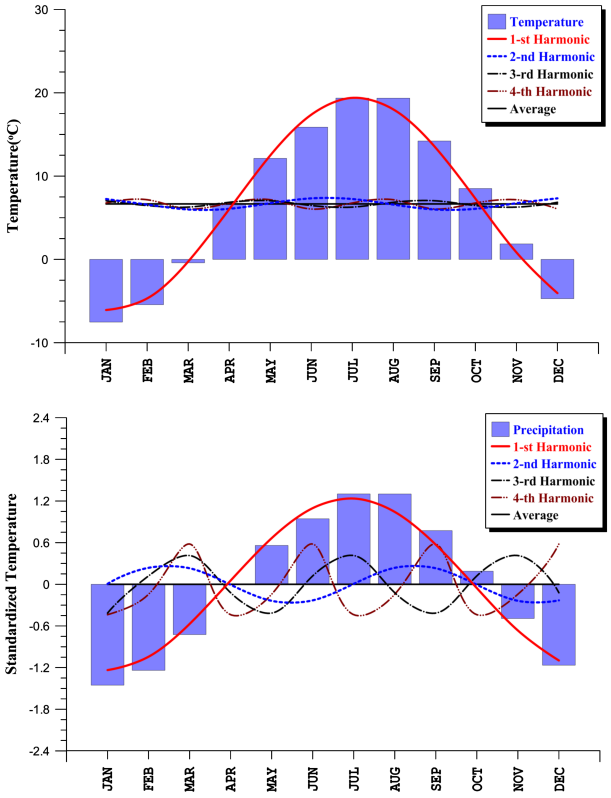

Figure 3. An example illustrating the interpretation of the annual cycle at a station with pronounced warm season. Left figure is the harmonic fit of monthly temperature and right one is the harmonic fit of standardized temperature index (STI) of Yeosu station applied in this study.

trigonometric functions. Harmonic analysis applied first in investigating the climatic temperature regimes by Horn and Bryson (1960) has been considered as an objective and analytic approach to examine seasonality of climatic variables. Figure 3 shows an example of four harmonics for annual variation based on the study of Scott and Shulman (1979), and the sample harmonic fits for the same period using the STI previously converted from original temperature data. According to the assumption that the only one maximum or minimum value of temperature data is corresponded to the extreme ENSO forcing, the first harmonic is derived from the idealized 2-year ENSO composite with the amplitude and phase of the ENSO-related temperature signal. In this first harmonic curve, the amplitude indicates the representative magnitude of the temperature response to ENSO events, and the phase angle refers to the time showing a maximum departure from the mean value in the first harmonic cycle (Figure 4). The first harmonic is fitted as follows based on Wilks (1995):

$$X_t = \overline{X} + \sum_{k=1}^{N/2} \left[C_k \cos\left(\frac{2\pi kt}{N} - \emptyset_k \right) \right]$$
$$= \overline{X} + \sum_{k=1}^{N/2} \left[A_k \cos\left(\frac{2\pi kt}{N} \right) + B_k \sin\left(\frac{2\pi kt}{N} \right) \right] \quad (1)$$

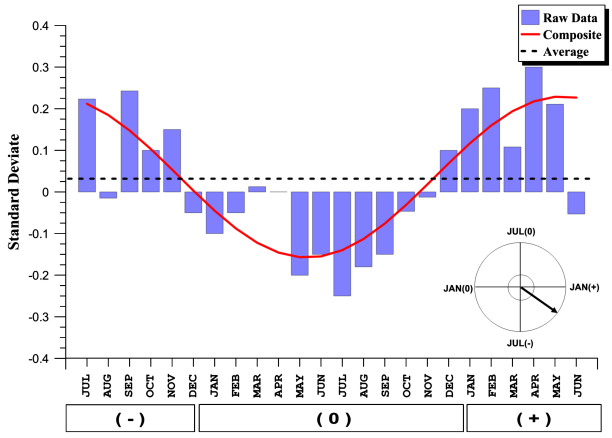

Figure 4. A first harmonic fit to the temperature El Niño composite for the Yeosu station. The amplitude and the phase of the first harmonic are presented as a harmonic dial.

where

$$A_k = \frac{2}{N}\sum_{t=1}^{N} X_t \cos\left(\frac{2\pi kt}{N}\right) \tag{2}$$

$$B_k = \frac{2}{N}\sum_{t=1}^{N} X_t \sin\left(\frac{2\pi kt}{N}\right) \tag{3}$$

where X_t is the STI value at time t. observation, $\overline{X}$, is the mean value of the STI, k is the harmonic number (the first harmonic, k = 1), N. the sample size (period), C_k is the maximum deviation from the mean value, $\emptyset_k$ is the time when the harmonic has a maximum, and A_k and B_k are the Fourier coefficients. The terms C_k and $\emptyset_k$ represent the amplitude and the phase shift of the harmonic, given by

$$C_k = \left(A_k^2 + B_k^2\right)^{0.5} \tag{4}$$

and

$$\phi_k = \begin{cases} \tan^{-1}\frac{B_k}{A_k}, & A_k > 0 \\ \tan^{-1}\frac{B_k}{A_k} \pm \pi, \quad or \pm 180°, & A_k < 0 \\ \frac{\pi}{2}, \ or \ 90°, & A_k = 0 \end{cases} \tag{5}$$

The information included in harmonic curves can be effectively summarized as a graphical device known as the harmonic dial, which is useful for representing the geographic trends of periodic parameters. The first harmonic is expressed as a vector having the length and direction (angular orientation), which represent the intensity and timing of the maximum response of the ENSO forcing to the temperature patterns, respectively, and then is represented as a harmonic dial (Hsu and Wallace, 1976). According to the map of harmonic dials, the 'candidate regions' showing spatially coherent ENSO-related temperature signal are identified.

The harmonic dials are useful to identify the candidate regions by detecting a group of vectors having the similar strength and direction, but are not sufficient to clearly identify the consistency of the ENSO–temperature relationship. The spatial coherence is employed to determine the candidate regions having coherent harmonic vectors, and is estimated through the following calculation based on the study of Ropelewski and Halpert (1986, 1987) and Kahya and Dracup (1993):

$$C = \frac{[V]}{S} \tag{6}$$

$$[V] = \frac{\left[\left(\sum V\cos\theta\right)^2 + \left(\sum V\sin\theta\right)^2\right]^{1/2}}{L}, \quad S = \frac{\sum V}{L} \tag{7}$$

where $[V]$ is the average vector of the individual components of the harmonic vectors in the proposed candidate regions, S is the average of the individual vector magnitudes, V is the magnitude of the vector, θ is the angular orientation of the vector, and L is the total number of vectors within the regions. The coherence of zero indicates that a group of vectors show the same magnitude in different directions, while the value of one refers to that all vectors have the same direction, but do not necessarily all have the same magnitude (Brooks and Carruthers, 1953). According to the suggestion of Halpert and Ropelewski (1992), a candidate region is identified under the condition that the value of spatial coherence is larger than 0.85.

With a view to detect the ENSO-related signal season showing the consistent and apparent response of the ENSO forcing to the temperature patterns, the aggregate composites are formed by spatially averaging the entire ENSO composites within each candidate region. The aggregate composites are plotted based on a 36-month period following the approach of Kahya and Dracup (1993), to detect more accurately the signal season and to cover the entire life cycle of the ENSO events.

According to the aggregate composite, only one season within the ENSO cycle based on the aforementioned assumption that the first harmonic has one maximum and minimum values during the ENSO cycle is detected by means of searching a group of anomalies having the same signal for more than four consecutive months at least. Taking the distance between the tropical Pacific Ocean and the study area located in the mid-latitude into consideration, it is reasonable to regard the responding period of ENSO forcing as the event year and the subsequent year of the event.

In order to examine the consistency of the ENSO-related temperature signal and calculate the correlation between the ENSO forcing and temperature patterns, another time series of the monthly temperature values is employed based on the candidate regions and detected seasons previously obtained from the aggregate composites. These ITS are formed not only by regional average of the temperature data over the all stations, but also by temporal average for all years of record.

Finally, for the purpose of determining a core regions, which is defined as a region having a strong and consistent temperature responses to the ENSO episodes, within the candidate regions previously detected from the harmonic dial, the rate of temporal consistency is calculated based

on the proportion of number of years in the ITS having the ENSO-related temperature signal to the number of total ENSO years.

Ropelewski and Halpert (1986) examined the occurrence of extreme temperature events with relation to the ENSO-related temperature response to check the climatic link between the ENSO phenomena and the extreme phase of temperature. Following this context, in this study the number of extreme temperature occurrences in association with ENSO episodes during the signal season is counted. In order to assign the limits of the level, the ITS values are ranked from the largest amount to the smallest amount, normalized by the amount of the total data, and then obtained the probability from the Weibull plotting position formula. The highest level is designated with the probability of ITS equal to 80%, while the lowest level with the probability of ITS equal to 20% (Kahya and Dracup, 1994).

2.2.3. *Comparative analysis and interpretation*

As an effective method of assigning the significance level of the ENSO–temperature relationship, the hypergeometric distribution test is employed, which is a statistical approach calculating the probability of a random occurrence of the signal season during the ENSO event. Haan (1977) calculated 'the cumulative probability that at least m successes are obtained in n trials from a finite population of size N containing k successes' using the hypergeometric distribution test. In this study, the test is carried out in two cases (A and B) according to the definition of a success. For the ENSO–temperature relationship, a success means the occurrence of an ITS value above (below) the median in case A, while a success means that of a warmest (coldest) ITS value larger (smaller) than 80% (20%) value in case B, following the suggestion of Kahya and Dracup (1994).

The annual cycle analysis on the basis of the approach of Kahya and Dracup (1993) and Karabörk and Kahya (2003) is applied to compare the signal seasons of the warm and cold episodes in terms of the intensity and trend of the response. In this analysis, the monthly temperature data are converted to a modular coefficient, which is obtained by the proportion of the original temperature data to the monthly mean data averaged over the total data series. These resulting data sets place all stations on a same basis with invariable condition of the cyclic feature of the values, and are checked whether the El Niño/La Niña forcings modulate the temperature patterns by increasing or decreasing.

For the purpose of checking a significant difference in the magnitude of the both extreme phase-related temperature signals, a statistical hypothesis test using the Mann–Whitney U approach is carried out. The two data sets are collected regarding the extreme phase of ENSO (corresponding to El Niño/La Niña episodes, respectively), and then the null hypothesis is assumed as the equality of the two data sets. According to the result of the rank-sum hypothesis test, the quantitative and noticeable difference between the two data sets can be identified.

As another comparative method for the El Niño/La Niña-related temperature signals, the cross-correlation analysis is employed on the basis of seasonal comparison between the large-scale climate index (SOI) as an indicator of the ENSO forcing and the seasonal temperature data over South Korea. In order to minimize the problem such as spatial disparities over the stations and periodicities in the time series, the seasonal temperature data are transformed into non-exceedance probability time series. In addition, as a follow-up to the work Jin *et al.* (2005), the seasonal SOI is classified into five categories based on the SO phases, e.g. extreme, moderate, and neutral phase of the SO, because without the categorization of the SOI data, no significant correlation was found. A more detailed explanation of the analysis was given in the first stage of data processing. These resulting CCC are used to examine the intensity and the trend (e.g. positive or negative response) of the ENSO–temperature correlation.

3. Results and discussion

3.1. El Niño–temperature relationship

Figure 5 shows the results of detecting the candidate regions based on a harmonic dial map resulting from the composite and harmonic analyses. The harmonic dial

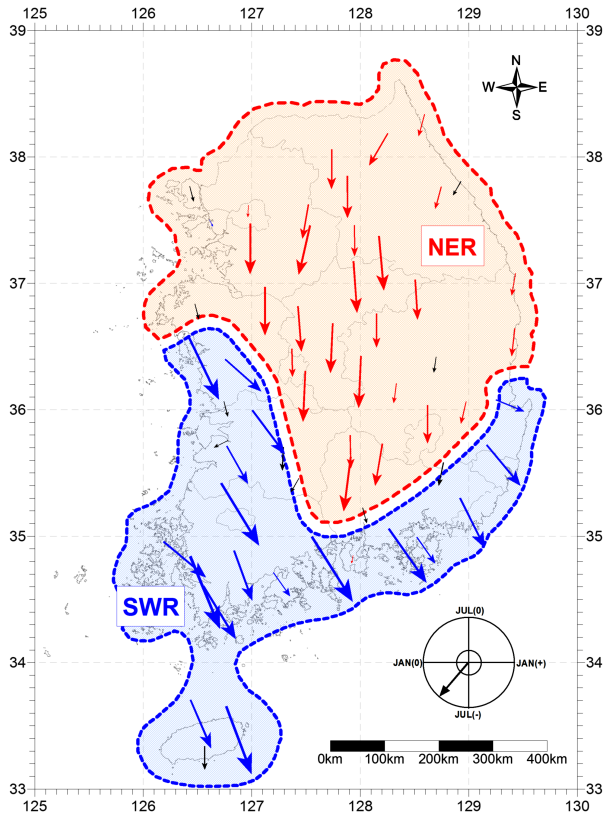

Figure 5. Temperature vectors based on the 24-month harmonic fitted to El Niño composites. Scale for the direction of arrows: south, July(−); west, January(0); north, July(0); and east, January(+). The magnitude of arrows is proportional with the amplitude of the harmonics.

map is plotted in the form of vector having the length and angular orientation (direction), which refer to the amplitude and phase of the idealized 2-year ENSO composite cycle representing the ENSO-related temperature response, respectively. According to the harmonic dial map, the overall study area is grouped into two candidate regions, namely from north to south: the north-east region (NER) and the south-west region (SWR). The difference of vectorial patterns in these regions can be attributed to the different amplitude and phase of the maximum departure from the composite mean in the first harmonic cycle extracted from each region, in which the ENSO responses differ in timing, intensity, and extent. For these candidate regions, the overall results of determining the core region using the rate of temporal consistency are shown in Table 2.

3.1.1. *North-east region*

The NER region has a spatial coherence of 0.95. In Figure 6(a), the aggregate ENSO composite of the NER region indicates a tendency for below normal temperature, i.e. smaller than the 50% value, during the July (0) to October (0), while a tendency for above normal temperature during the November (0) to April (+). The period outlined by the dashed lines represents the season having a significant ENSO-related temperature signal. The ITS for the previously identified season show that seven out of ten El Niño episodes are associated with cold/warm conditions at a consistency rate of 0.70 as described in Figure 6(b) and (c). Based on the highest limit (80%) and lowest limit (20%) for the ITS values, which is drawn by the dashed lines in Figure 6(b) and (c), three/two of eight extremely cold/warm temperature occurrences are associated with the El Niño episodes. It is evident from the results presented here that the NER region is evaluated as a core region with a coherent and consistent El Niño–temperature relationship.

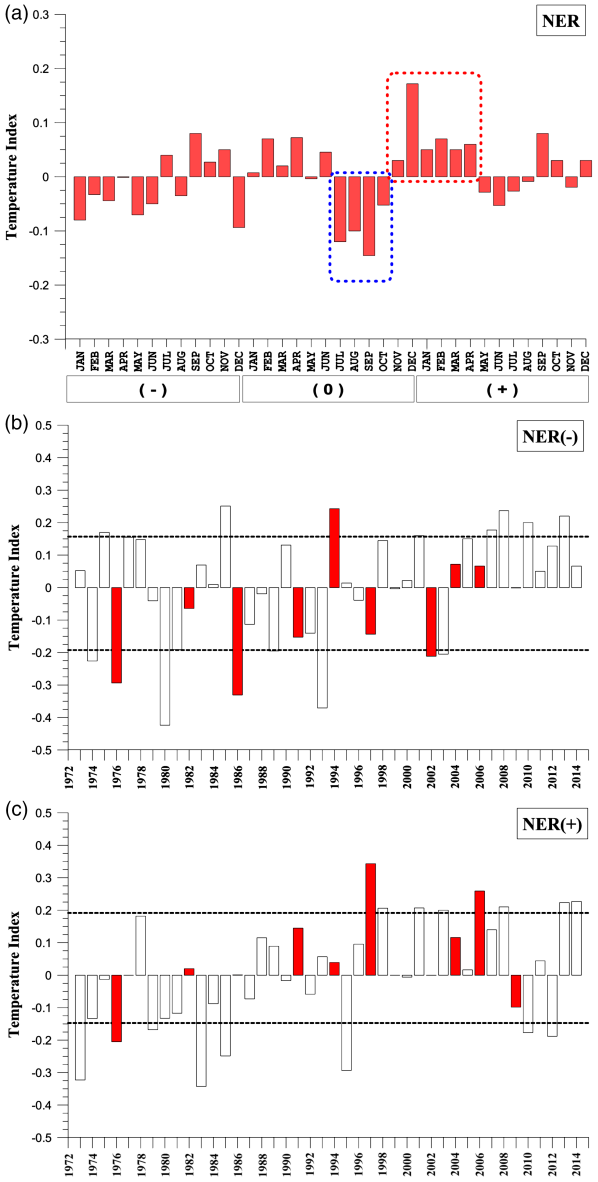

Figure 6. (a) El Niño aggregate composite for the candidate NER region. The dashed line box delineates the season of possible El Niño-related responses. The index time series for the NER region for (b) the cold season of negative signal previously detected [refer to the lower dashed box in (a)] and (c) the warm season of positive signal previously detected [refer to the upper dashed box in (a)]. El Niño years are shown by solid bars. The dashed horizontal lines are the upper (80%) and lower (20%) limits for the distribution of ITS values.

3.1.2. *South-west region*

The coherence value of the SWR region is 0.97. The aggregate ENSO composite of the SWR region shows that colder conditions are related to the El Niño phenomena for the June (0) through October (0), while warmer conditions are associated with the El Niño event for the November (0) through April (+) as shown in Figure 7(a), in which the period outlined by the dashed lines indicates the season having ENSO–temperature response. The ITS for the signal season reveals that seven/eight out of ten warm episodes represent the cold/warm season indicating a relatively high rate of consistency (0.70/0.80) as shown in Figure 7(b) and (c). Three/two out of eight occurrences

Table 2. Properties of the candidate regions (El Niño events).

Region	Coherence	Response	Season	Total episode	Occurrence episode	Consistency	Extreme events
NER	0.95	Cold	July(0)–October(0)	10	7	70%	3
		Warm	November(0)–April(+)	10	7	70%	2
SWR	0.97	Cold	June(0)–October(0)	10	7	70%	3
		Warm	November(0)–April(+)	10	8	80%	2

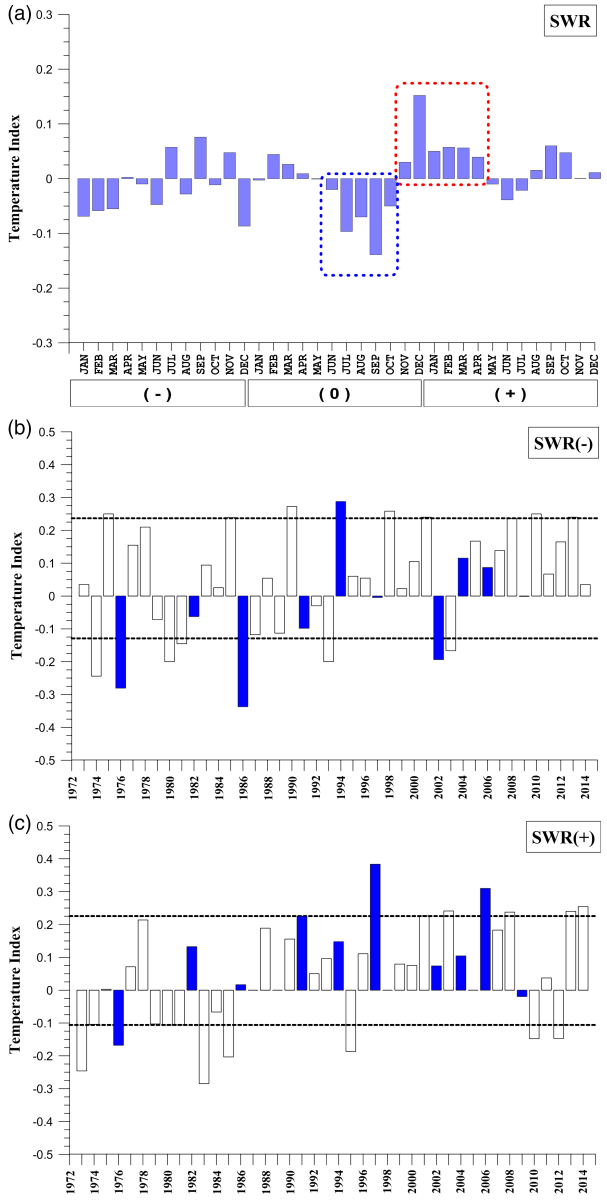

Figure 7. (a) El Niño aggregate composite for the candidate SWR region. The dashed line box delineates the season of possible El Niño-related responses. The index time series for the SWR region for (b) the cold season of negative signal previously detected [refer to the lower dashed box in (a)] and (c) the warm season of positive signal previously detected [refer to the upper dashed box in (a)]. El Niño years are shown by solid bars. The dashed horizontal lines are the upper (80%) and lower (20%) limits for the distribution of ITS values.

of coldest/warmest years with values of equal to or larger (smaller) than 80% (20%) value, are associated with the El Niño episodes, using the highest and lowest limits for the ITS values, which is drawn by the dashed lines in Figure 7(b) and (c). It is clear from these results that the SWR region is considered as a core region with a strong and consistent relationship between the warm episode of ENSO and temperature patterns.

3.2. La Niña–temperature relationship

As a result of searching the candidate regions, a harmonic dial map based on the composite and harmonic analyses is

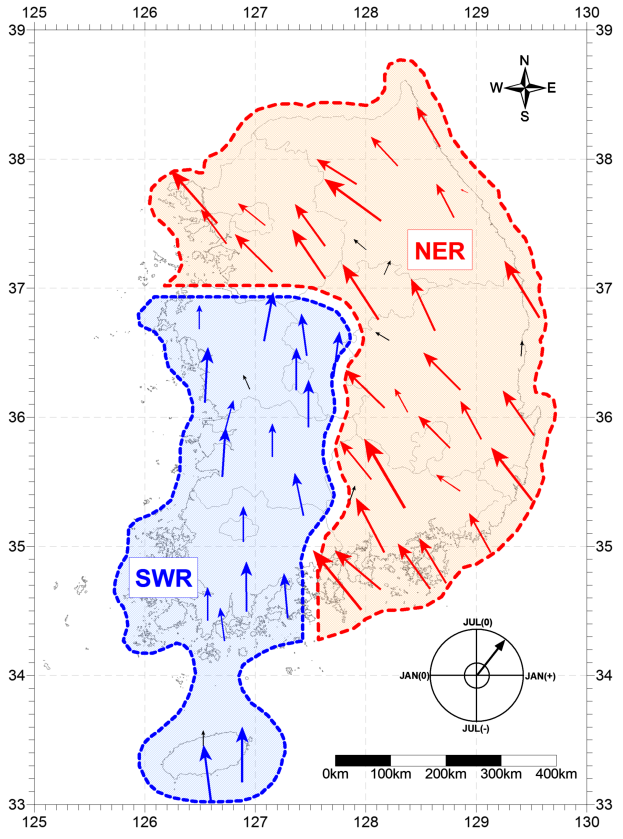

Figure 8. Temperature vectors based on the 24-month harmonic fitted to La Niña composites. Scale for the direction of arrows: south, July(−); west, January(0); north, July(0); and east, January(+). The magnitude of arrows is proportional with the amplitude of the harmonics.

shown in Figure 8. In the harmonic dial map, two candidate regions, namely from north to south: the NER and the SWR are detected. For these candidate regions, the overall results of determining the core region using the rate of temporal consistency are shown in Table 3.

3.2.1. *North-east region*

The spatial coherence of the NER region is equal to 0.98. In Figure 9(a), the aggregate ENSO composite of the NER region indicates a tendency for above normal temperature, i.e. larger than the 50% value, during the June (0) to October (0), while a tendency for below normal temperature during the November (0) to February (+). The range outlined by the dashed lines represents the season having a significant ENSO-related temperature signal. The ITS for the previously identified season show that nine/seven out of nine La Niña episodes are associated with warm/cold conditions at a consistency rate of 1.00/0.78 as described in Figure 9(b) and (c). Based on the highest limit (80%) and lowest limit (20%) for the ITS values, which is drawn by the dashed lines in Figure 9(b) and (c), three of eight extremely warm/cold temperature occurrences are associated with the cold phase of SO. It is evident from the results presented here that the NER region is evaluated as a core region with a coherent and consistent La Niña–temperature relationship.

Table 3. Properties of the candidate regions (La Niña events).

Region	Coherence	Response	Season	Total episode	Occurrence episode	Consistency	Extreme events
NER	0.98	Warm	June(0)–October(0)	9	9	100%	3
		Cold	November(0)–February(+)	9	7	78%	3
SWR	0.99	Warm	July(0)–October(0)	9	8	89%	4
		Cold	November(0)–April(+)	9	7	78%	3

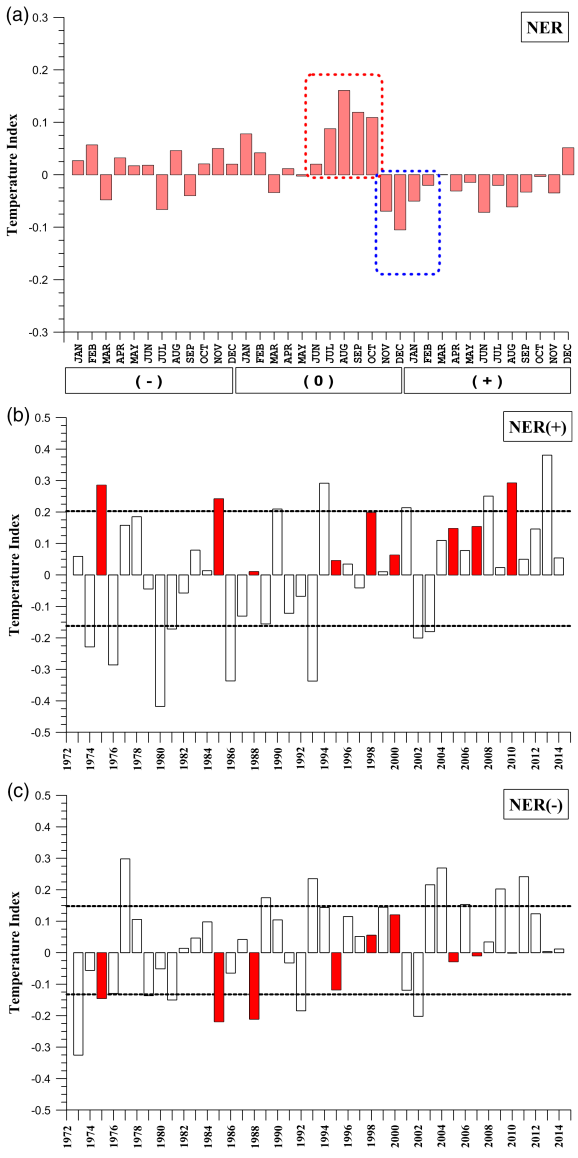

Figure 9. (a) La Niña aggregate composite for the candidate NER region. The dashed line box delineates the season of possible La Niña-related responses. The index time series for the NER region for (b) the warm season of positive signal previously detected [refer to the upper dashed box in (a)] and (c) the cold season of negative signal previously detected [refer to the lower dashed box in (a)]. La Niña years are shown by solid bars. The dashed horizontal lines are the upper (80%) and lower (20%) limits for the distribution of ITS values.

3.2.2. South-west region

The coherence value of the SWR region is 0.99. The aggregate ENSO composite of the SWR region shows that warmer conditions are related to the La Niña phenomena for the July (0) through October (+), while colder conditions are associated with the La Niña event for the November (0) through April (+) as shown in Figure 10(a), in which the period outlined by the dashed lines indicates the season having ENSO–temperature response. The ITS for the signal season reveals that eight/seven out of nine La Niña events represent the warm/cold season indicating a reasonable rate of consistency (0.89/0.78) as shown in Figure 10(b) and (c). Four/three out of eight occurrences of warmest/coldest years with values of equal to or larger (smaller) than 80% (20%) value, are associated with the La Niña episodes, using the upper and lower limits for the ITS distribution values, which is drawn by the dashed lines in Figure 10(b) and (c). It is therefore plausible to suggest that the SWR region is considered as a core region with a strong and consistent relationship between the La Niña and temperature patterns.

3.3. Comparative analysis of El Niño and La Niña

Table 4 shows the results of calculating the probability of a random occurrence of the signal season during the warm episodes based on the hypergeometric distribution test. In case A, all regions indicate a statistically significant relationship with a high significance level (between 92 and 99%), based on a very low chance of random occurrence of the ITS value above/below the median for the El Niño events. Additionally, in case B, based on a very low chance of random occurrence of the driest/warmest ITS value smaller/larger than 20/80% value for the El Niño events, the relationship of all regions result in a rate of 69% for the cold response and 87% for the warm response. On the other hand, the results of calculating the probability during the cold events using the hypergeometric distribution model are shown in Table 5. The relationships of the both regions for case A are found to be highly significant at the 86–99%, considering very low chance of random occurrence of the ITS value below/above the median for the La Niña events. In case B, the SWR warm case shows a highly significant relationship with a 97% significance level, based on a very low chance of random occurrence of the warmest ITS value lager than 80% value for the La Niña events, while the rates of the other cases are calculated as 87%. Thus, the analyses for the two extreme events show the similar results indicating a high statistical significance level for the above/below normal temperature.

Figure 11 illustrates the relationship between the El Niño composite cycle and the annual temperature cycle

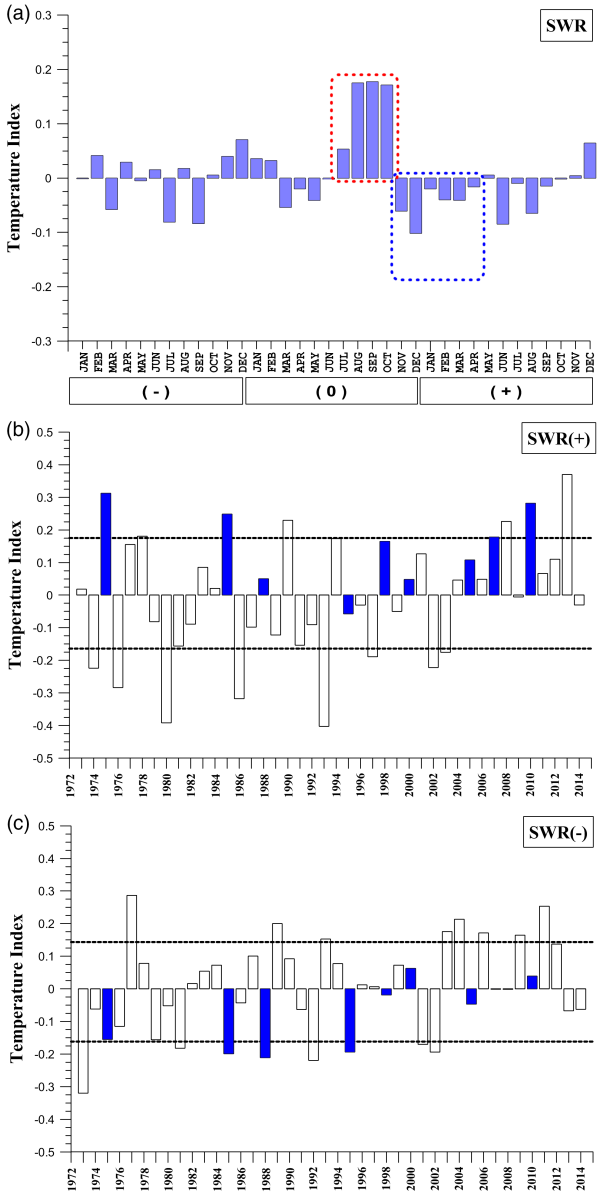

Figure 10. (a) La Niña aggregate composite for the candidate SWR region. The dashed line box delineates the season of possible La Niña-related responses. The index time series for the SWR region for (b) the warm season of positive signal previously detected [refer to the upper dashed box in (a)] and (c) the cold season of negative signal previously detected [refer to the lower dashed box in (a)]. La Niña years are shown by solid bars. The dashed horizontal lines are the upper (80%) and lower (20%) limits for the distribution of ITS values.

plotted by modular coefficients. Since a consecutive below/above normal temperature period for the El Niño signal season is detected in the El Niño–annual temperature cycle, it is plausible that the El Niño forcing modulates temperature by decreasing–increasing pattern its magnitude in the NER and SWR region, respectively. Based on the conversion of temperature date into modular coefficients, the relationship between the La Niña composite cycle and the annual temperature cycle are shown in Figure 12. There exists a group of persistent above/below normal temperature for the La Niña signal season in the La Niña–annual temperature cycle, therefore

Table 4. Probabilistic assessments for significance level based on the hypergeometric distribution which is used to determine the cumulative probability that at least m successes are obtained in n trials from a finite population of size N containing k successes (El Niño events).

Case	Region	Response	N	k	n	m	Probability
A	NER	Cold	42	18	10	7	0.043
		Warm	42	20	10	7	0.081
	SWR	Cold	42	15	10	7	0.012
		Warm	42	24	10	8	0.076
B	NER	Cold	42	8	8	3	0.132
		Warm	42	8	8	2	0.319
	SWR	Cold	42	8	8	3	0.132
		Warm	42	8	8	2	0.319

Table 5. Probabilistic assessments for significance level based on the hypergeometric distribution which is used to determine the cumulative probability that at least m successes are obtained in n trials from a finite population of size N containing k successes (La Niña events).

Case	Region	Response	N	k	n	m	Probability
A	NER	Warm	42	27	9	9	0.010
		Cold	42	16	9	6	0.047
	SWR	Warm	42	22	9	8	0.143
		Cold	42	20	9	7	0.040
B	NER	Warm	42	8	8	3	0.132
		Cold	42	8	8	3	0.132
	SWR	Warm	42	8	8	4	0.027
		Cold	42	8	8	3	0.132

it is reasonable that the La Niña forcing modulates temperature by increasing–decreasing pattern its magnitude in the NER and SWR region, respectively. According to the above results of the annual cycle analyses, El Niño forcing modulates temperature by suppressing–enhancing pattern, while La Niña forcing modulates temperature by enhancing–suppressing pattern for the signal seasons.

Based on the statistical hypothesis test by the Mann–Whitney U approach, the quantitative and noticeable difference between the two data sets of the warm and cold episodes was identified with the rate of significant relationship up to 75%. According to the above results, at the 0.10 significance level, there is enough evidence to suggest that average value of signal season associated with the warm episodes is different from (larger than) those in association with the cold episodes.

The results of calculating CCC to examine the intensity and the trend of the ENSO–temperature correlation are shown in Table 6 and Figure 13, on the basis of seasonal comparison between the large-scale climate index (categorized SOI) and the monthly temperature data (non-exceedance probability). As the coverage and number of stations included the NER and the SWR regions previously identified as 'Core Region' by the composite and harmonic analyses for the El Niño episodes are different from those for the La Niña episodes, the results of cross-correlation analysis are expressed with respect to the

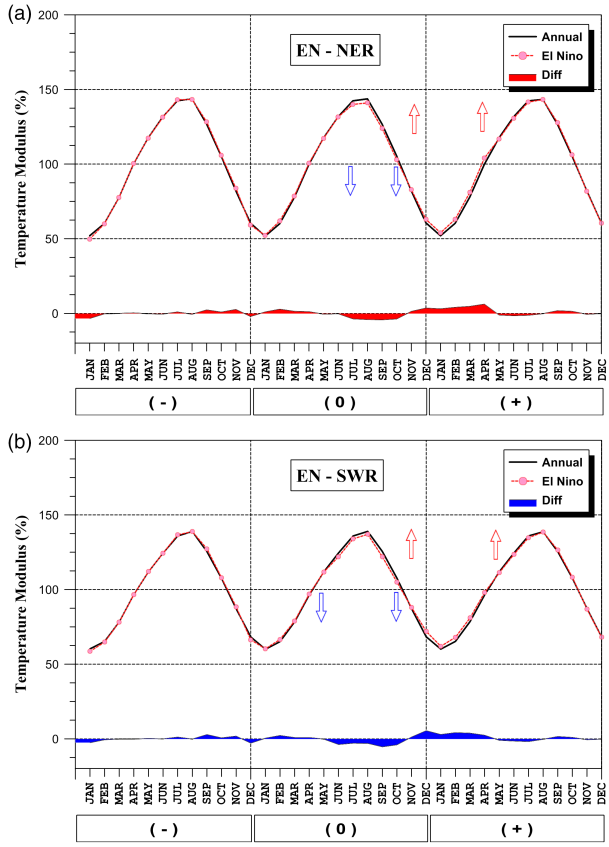

Figure 11. The comparison of El Niño composite cycles (shown by dashed line) and annual cycles (shown by solid line) of (a) the NER and (b) SWR, based on modular coefficients. Arrows indicate the beginning and end months of the SO signal season.

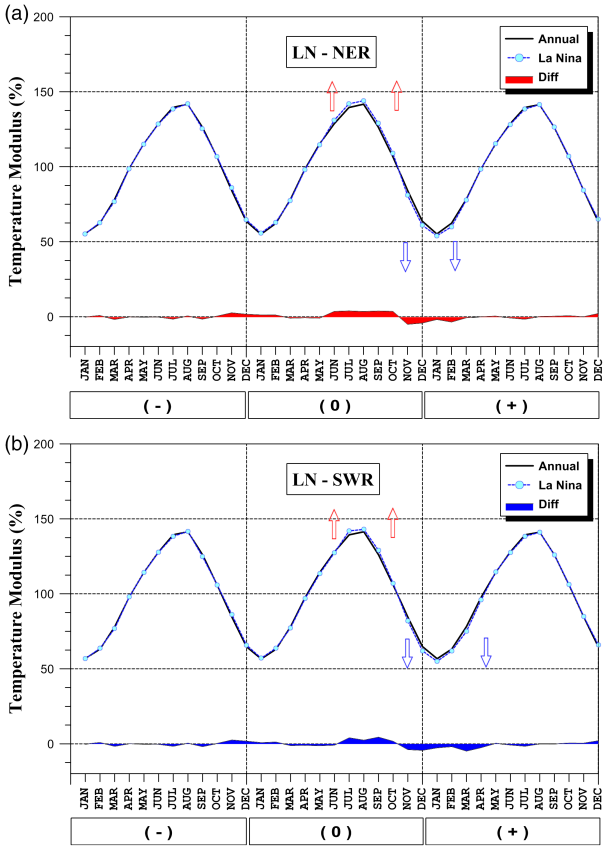

Figure 12. The comparison of La Niña composite cycles (shown by dashed line) and annual cycles (shown by solid line) of (a) the NER and (b) SWR, based on modular coefficients. Arrows indicate the beginning and end months of the SO signal season.

both extreme phases of ENSO. As a general result, the both analyses for two extreme phases of SO show significant correlations with the non-exceedance probability time series for the 0.05 significance level. The strongest correlation coefficients (0.66–0.95) with the lag-4 seasons are calculated at all core regions under the Strong El Niño SOI condition and the highest rate of correlation coefficients (0.50–0.67) with the lag-3 seasons are found at all core regions under the Strong La Niña condition (see the underlined values in Table 6). As a result, the stronger intensity of the ENSO forcing, the larger impact of temperature at overall South Korea with lag time 3 and 4 seasons.

3.4. Discussion

According to the global scale study by Halpert and Ropelewski (1992) regarding the ENSO–temperature teleconnection, conclusive findings of eastern Asia are not clearly documented due to the scarcity of quantitative temperature data of stations for this region including South Korea, which is insufficient to analysis the remote influence. Based on a careful visual inspection of harmonic dial map of the above global scale study, several harmonic vectors are plotted without any consistent magnitude and phase angle because of the limitation of temperature data. This present study provides better insights and a substantial amount of information on the ENSO–temperature teleconnections over a part of eastern Asia region that has not been carried out by the previous studies. In more regionally focused findings of the previous study, Halpert and Ropelewski (1992) documented that temperature anomalies over northwest North America as well as Japan (mid-latitude area) during cold events show negative anomalies during the northern winter and spring. These results are consistent with the outcomes of this present study of the signal seasons which show the below normal temperature associated with the high phase of SO in the both core regions.

Taking methodology into consideration, Jin *et al.* (2005) identified statistically significant correlations between the extreme phases of SO and Korea–Japan precipitation patterns based on the cross-correlation analysis using the categorized SOI classified by five groups according to their magnitudes. While they pointed out significant correlations (−0.61) between the strong La Niña SOI and precipitation in Busan station located in southernmost part of the study area, the correlation coefficients from this present analysis are calculated as 0.50–0.67 under the strong La Niña SOI condition and 0.66–0.95 under the strong El Niño SOI condition on an average basis over the all core regions. The differences of the two analyses are attributed to the date scale and areal coverages for stations (1:60).

Table 6. Cross-correlation coefficients with respect to regions.

Core region		Strong El Niño SOI				Normal condition				Strong La Niña SOI			
		lag-1	lag-2	lag-3	lag-4	lag-1	lag-2	lag-3	lag-4	lag-1	lag-2	lag-3	lag-4
El Niño	NER	−0.11	−0.16	−0.04	0.91	0.11	0.16	0.03	−0.07	−0.18	0.12	0.60	0.06
	SWR	−0.18	0.09	−0.18	0.66	0.09	0.11	0.11	0.02	−0.13	0.01	0.50	0.01
La Niña	NER	−0.15	−0.03	−0.09	0.77	0.11	0.14	0.08	−0.02	−0.18	0.01	0.52	0.04
	SWR	−0.21	−0.02	−0.07	0.95	0.11	0.13	0.00	−0.07	−0.21	0.13	0.67	0.01

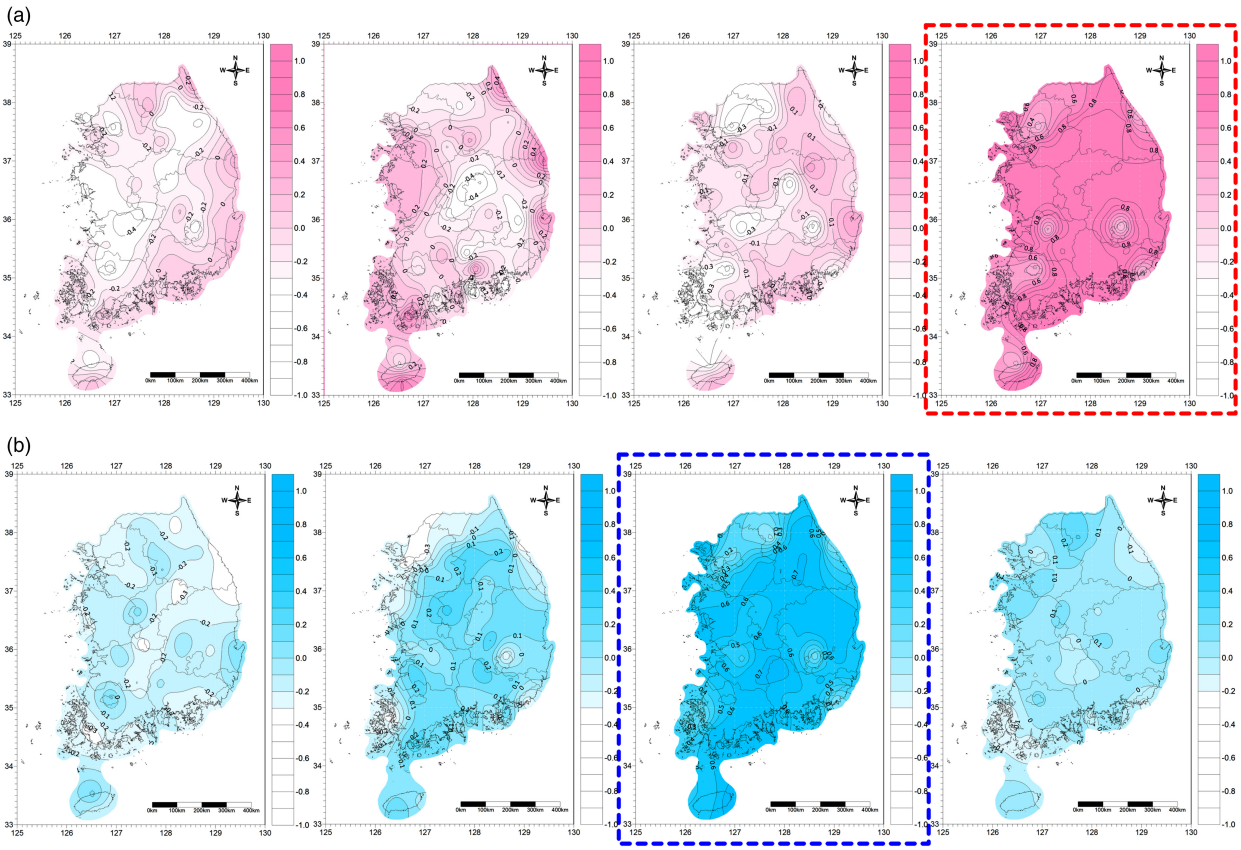

Figure 13. Contour maps of CCC between the seasonal temperatures and the categorized SOI series at different lags (from left to right, lag-1, lag-2, lag-3, and lag-4) for (a) Strong El Niño and (b) Strong La Niña.

In comparison with several recent studies concerning the ENSO–temperature relationship over South Korea, the overall outcomes are in agreement with the findings of Cha *et al.* (1999) with respect to positive/negative signals during El Niño/La Niña events. They pointed out that El Niño forcing has a tendency to modulate the temperature over Korea by enhancing or suppressing with respect to seasons. Also, the below/above normal temperature for all core regions based on the aggregate composites of this analysis, coincides with the results of Kang (1998) and Min and Yang (1998) in terms of the tendency for negative/positive response for the warm event in summer/winter.

As a general result, the overall findings of this diagnostic study are thought to provide additional confirmation to the climatic relationship between ENSO forcing and hydrometeorological fluctuations over mid-latitude area.

4. Summary and conclusion

In this investigation, the remote impacts of the extreme phases of the SO, i.e. El Niño and La Niña events, on the monthly temperature patterns over South Korea are examined based on the composite and harmonic analyses. The overall results of the ENSO–temperature teleconnections are summarized as follows, with the details of the analysis shown in Table 2 and Table 3. According to the composite and harmonic analysis, the two core regions, namely the NER and the SWR, were determined with a high level of the spatial coherence and temporal consistency rate, which represent the geographical extent and magnitude of the response of the ENSO forcing to the temperature patterns.

The main conclusions of this investigation are:

(1) El Niño–temperature relationships: the temperature anomalies are below normal for summer through fall of the ENSO year and above normal for winter through spring of the following year. The negative signal

seasons are July(0)–October(0) for NER and June(0)–October(0) for SWR, while the positive signal seasons are November(0)–April(+) for both regions. The spatial coherence rates of NER and SWR for El Niño events are 0.95, 0.97 and the temporal consistency rates of each region for the warm episodes are 0.70/0.70 (cold/warm) and, 0.70/0.80 (cold/warm), respectively.

(2) La Niña–temperature relationships: According to the harmonic analysis, the apparent signal season for the warm and cold period are June(0)–October(0) and November(0)–February(+) for NER, and July(0)–October(0) and November(0)–April(+) for SWR. In other words, the temperature anomalies for the both regions are above normal for summer through fall of the ENSO year and below normal for winter through spring of the following year. The spatial coherence rates of NER and SWR are 0.98 and 0.99 and the temporal consistency rates of the each core regions for the cold events are 1.00/0.78 (warm/cold) and 0.89/0.78 (warm/cold), respectively.

(3) A comparative analysis between El Niño– and La Niña–temperature relationships reveals the similar results indicating a high statistical significance level for the above/below normal temperature with reverse patterns of sign, i.e. negative–positive and positive–negative responses, respectively. These transitional responses imply that the proposed area located in mid-latitude, relatively remote from the central-eastern tropical Pacific Ocean, could be considered as an edge of the scope influenced by ENSO forcing. Moreover, the cold–warm pattern anomalies during the warm event years are more remarkable and significant than the warm–cold departures during the cold event years according to the results of the comparative analyses. Based on the annual cycle analysis, El Niño forcing modulates temperature by decreasing-increasing pattern, while La Niña forcing modulates temperature by enhancing–suppressing pattern for the signal seasons. Additionally, Mann–Whitney U hypothesis test implies that the average value of signal season associated with the warm episodes is larger than those in association with the cold episodes. Finally, the overall outcomes of cross-correlation analysis between the seasonal temperature and the categorized SOI confirm the implied teleconnections between the tropical SO phenomenon and temperature over South Korea, with the high value of correlation of a lag time of 3 and 4 seasons.

Finally, the climatic teleconnections between the extreme phase of SO and mid-latitude temperature are identified over South Korea.

References

Ahn JB, Ryu JH, Cho EH, Park JY. 1997. A study of correlations between air-temperature and precipitation in Korea and SST over the tropical Pacific. *J. Korean Meteorol. Soc.* **33**: 487–495 (in Korean).

Berlage HP. 1966. *The Southern Oscillation and World Weather*, Vol. **88**. Royal Dutch Meteorological Institute: De Bilt, The Netherlands, 152 pp.

Bradley RS, Diaz HF, Kiladis GN, Eischeid JK. 1987. ENSO signal in continental temperature and precipitation records. *Nature* **327**: 487–501.

Brooks CEP, Carruthers N. 1953. *Handbook of Statistical Methods in Meteorology*. Her Majesty's Stationery Office: London.

Cha EJ, Jhun JG, Chung HS. 1999. A study on characteristics of climate in South Korea for El Niño/La Niña years. *J. Korean Meteorol. Soc.* **35**: 98–117 (in Korean).

Guttman NB. 1998. Comparing the Palmer drought index and the standardized temperature index. *J. Am. Water Resour. Assoc.* **34**(1): 113–121.

Ha KJ. 1995. Interannual variabilities of wintertime Seoul temperature and the correlation with Pacific sea surface temperature. *J. Korean Meteorol. Soc.* **31**: 313–323 (in Korean).

Haan CT. 1977. *Statistical Methods in Hydrology*. Iowa State University Press: Ames, IA.

Halpert MS, Ropelewski CF. 1992. Surface temperature patterns associated with the Southern Oscillation. *J. Clim.* **5**: 557–593.

Horn LH, Bryson RA. 1960. Harmonic analysis of the annual march of precipitation over the United States. *Ann. Assoc. Am. Geogr.* **50**: 157–171.

Hsu CF, Wallace JM. 1976. The global distribution of the annual and semiannual cycles in precipitation. *Mon. Weather Rev.* **104**: 1093–1101.

Jin YH, Kawamura A, Jinno K, Berndtsson R. 2005. Quantitative relationship between SOI and observed precipitation in southern Korea and Japan by nonparametric approaches. *J. Hydrol.* **301**: 54–65.

Kahya E, Dracup JA. 1993. US streamflow patterns in relation to the El Niño/Southern Oscillation. *Water Resour. Res.* **29**(8): 2491–2503.

Kahya E, Dracup JA. 1994. The influences of Type 1 El Niño and La Niña events on streamflows in the Pacific southwest of the United States. *J. Clim.* **7**: 965–976.

Kang IS. 1998. Relationship between El-Nino and Korean climate variability. *J. Korean Meteorol. Soc.* **34**: 390–396 (in Korean).

Karabörk MÇ, Kahya E. 2003. The teleconnections between extreme phases of Southern Oscillation and precipitation patterns over Turkey. *Int. J. Climatol.* **23**: 1607–1625.

Kiladis GN, Diaz HF. 1989. Global climatic anomalies associated with extremes in the Southern Oscillation. *J. Clim.* **2**: 1069–1090.

Kiladis GN, van Loon H. 1988. The Southern Oscillation. Part VII: meteorological anomalies over the Indian and Pacific sectors associated with the extremes of the oscillation. *Mon. Weather Rev.* **116**: 120–136.

Lee DR. 1998. Relationships of El Niño and La Niña with both temperature and precipitation in South Korea. *J. Korea Water Resour. Assoc.* **31**(6): 807–819 (in Korean).

van Loon H, Madden R. 1981. The Southern Oscillation. Part I: global associations with pressure and temperature in northern winter. *Mon. Weather Rev.* **109**: 1150–1162.

McKee TB, Doesken NJ, Kleist J. 1993. The relationship of drought frequency and duration to time series. In *Proceedings of the 8th Conference on Applied Climatology*, Anaheim, CA, 179–187.

Min WK, Yang JS. 1998. A study on correlation between El-Nino and winter temperature and precipitation in Korea. *J. Korean Assoc. Reg. Geogr.* **4**(2): 151–164 (in Korean).

Quinn WH, Zopf DO, Short KS, Kuo Yang RTW. 1978. Historical trends and statistics of the Southern Oscillation, El Niño, and Indonesian droughts. *Fish. Bull.* **76**: 663–678.

Rasmusson EM, Carpenter TH. 1983. The relationship between eastern equatorial Pacific sea surface temperatures and rainfall over India and Sri Lanka. *Mon. Weather Rev.* **111**: 517–528.

Redmond KT, Koch RW. 1991. Surface climate and streamflow variability in the western United States and their relationship to large circulation indices. *Water Resour. Res.* **27**(9): 2381–2399.

Ropelewski CF, Halpert MS. 1986. North American precipitation and temperature patterns associated with El-Niño Southern Oscillation (ENSO). *Mon. Weather Rev.* **114**: 2165–2352.

Ropelewski CF, Halpert MS. 1987. Global and regional scale precipitation patterns associated with the El Niño/Southern Oscillation. *Mon. Weather Rev.* **115**: 1606–1626.

Ropelewski CF, Halpert MS. 1989. Precipitation patterns associated with the high index phase of the Southern Oscillation. *J. Clim.* **2**: 268–284.

Scott CM, Shulman MD. 1979. An areal temporal analysis of precipitation in the Northeastern United States. *J. Appl. Meteorol.* **18**: 627–633.

Trenberth KE. 1997. The definition of El Niño. *Bull. Am. Meteorol. Soc.* **78**: 2771–2777.

Walker GT. 1923. Correlation in seasonal variations of weather, VIII. A preliminary study of world weather. *Mem Indian Meteorol. Dept.* **24**: 75–131.

Walker GT, Bliss EW. 1932. World weather V. *Mem R. Meteorol. Soc.* **4**(36): 53–84.

Wilks DS. 1995. *Statistical Methods in Atmospheric Sciences*. Academic Press: London, UK, Chap. 8, 330–334.

WMO. 2014. El Niño/Southern Oscillation. WMO No. 1145, Geneva, Switzerland, 2–4.

